用いられている Gaussian03 を選択した．Gaussian03 は理論的には最も正確な予測が可能とされる非経験法に属するプログラムで，実験的には観測が難しい反応の中間体や遷移状態までも対象とすることができるため，量子化学の専門家のみならず実験系研究者にも広く利用されている．

2.2 計算モデル

計算に使用した粘土鉱物のモデルを図２に示す．このモデルは，Grim (1968)[5] を参考に２個の八面体シートとその上下を１２個の四面体が挟む２：１型の結晶構造で，ベントナイト主成分のスメクタイトの基本ユニットである．Gaussian03 による計算は，この単位ユニット表面に水分子１個が分布するモデルと陽イオン（Na^+，Ca^{2+}）を介して水分子が分布するモデルに対して行った．２：１型の粘土鉱物は，一般に負電荷が卓越するため層間および周囲に Na^+，Ca^{2+}などの陽イオンを吸着している．計算項目は，粘土鉱物の単位ユニット－水分子の構造最適化と結合エネルギーである．計算は，岩手大学情報処理センターの Altix3700 を利用し，RHF/6-31G(d, p) レベルで行った．

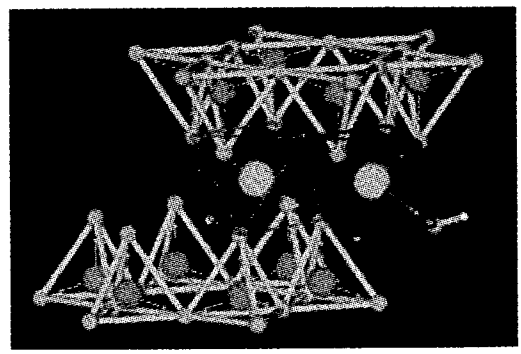

図２　計算に用いた粘土鉱物のユニットモデル

a. 構造最適化

構造最適化とは，分子にとって最も安定とされる構造を見つけることである．具体的には，分子構造を変えながらエネルギー計算を続け，より低いエネルギーを与える構造に収束するまで計算を行う．つまり，構造最適化とは，全エネルギーが極小となる分子構造を決定することである．本研究の場合，粘土表面に吸着する水分子の吸着構造を求めることになる．

b. 結合エネルギー計算

分子あるいは原子間の結合エネルギーは，化合物全体のエネルギーからそれらを構成する原子あるいは分子エネルギーの和を差し引くことによって求める．具体的には，系全体のポテンシャルエネルギーE_{HF}から，ある原子単独のポテンシャルエネルギーE_Fと他方の原子単独のポテンシャルエネルギーE_Hの和を差し引くことで結合エネルギーΔEを求める．本研究の場合，E_{HF}は粘土ユニットと水分子の和，E_Fは粘土ユニット，E_Hは水分子である．

$$\Delta E = E_{HF} - (E_F + E_H)$$

2.3 計算結果

a. 粘土鉱物と水分子の構造最適化

図３は粘土ユニットに水分子が直接分布する場合，図４(a)，(b)は陽イオン（Na^+，Ca^{2+}）を介して水分子が分布する場合の構造最適化の結果である．図３に示されたように水分子が単独で分布するときは，水素を粘土表面に向けて吸着する．２：１型の粘土鉱物は，ユニット全体として負電荷が卓越しているため，水分子の極性により正電荷を帯びた水素が吸着する．他の原子・分子に対する水分子の吸着方向は，２個ある水素のうち片方の水素だけを相手に向ける「線型」と両方の水素を向ける「対称型」があるが，粘土鉱物の場合，「対象型」である．

次に図４の陽イオンを介する場合は，粘土表面に吸着するのは陽イオンで，水分子は粘土表面ではなく陽イオンに吸着する．水分子の吸着方向は，陽イオンが正電荷なので負電荷を有する酸素である（水分子単独のときは水素）．図５は，原子を剛球とみなしたファンデルワールス半径（原子半径）で表示した図である．陽イオンは四面体シートの六員環（六角形の空間）の中に落ち込み，水素は陽イオンに少しめり込んでいる．両者とも強く吸着していることが分かる．

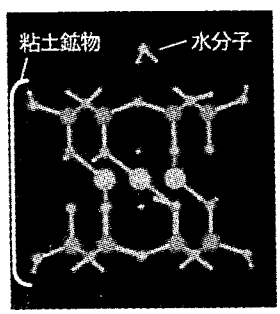

図３ 水分子が直接分布する場合の構造最適化の結果

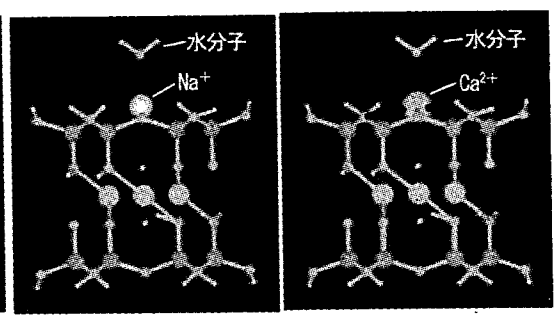

図４　陽イオンを介して水分子が分布する場合の構造最適化の結果

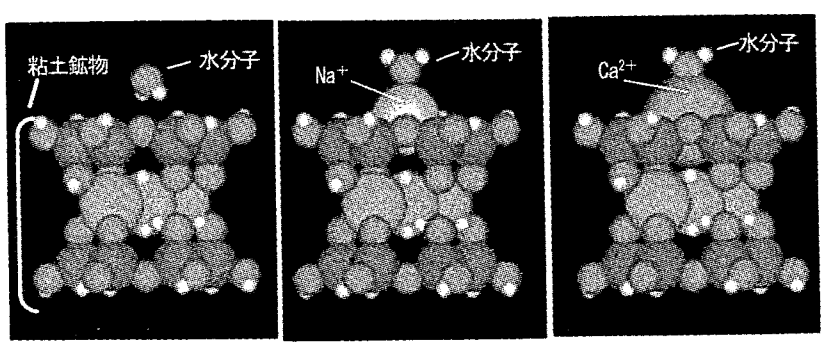

図５　粘土－水分子の構造最適化結果のファンデルワールス半径表示

b.粘土鉱物と水分子との結合エネルギー

表１に粘土鉱物と水分子との結合エネルギー計算結果を示す．マイナスの結合エネルギーは引力として，プラスは反発力として作用する．粘土表面と水分子に作用する力は，水分子単独，陽イオンがある場合にかかわらず全て引力である．水分子が単独で分布する場合の結合エネルギーは，⊿E ＝７．９kcal/mol で，オーダー的には水素結合の範囲である．水分子単独での吸着は非常に弱く，自由に動ける状態にある．これに対して陽イオン（Na^+, Ca^{2+}）を介して水分子が分布する場合の結合エネルギーは，陽イオンが Na^+のとき⊿E ＝１３．６kcal/mol，Ca^{2+}のとき⊿E ＝２９．３kcal/mol で，水素結合より強く，金属結合に近い状態にある．

表１　粘土鉱物と水分子との結合エネルギー

結合状態	結合エネルギー ΔE [kcal/mol]	
粘土－水分子	-7.908	
粘土－陽イオン－水分子	粘土－Na^+ -325.5	Na^+－H_2O -13.57
	粘土－Ca^{2+} -561.5	Ca^{2+}－H_2O -29.29

2.4 粘着力ｃに対する陽イオン，吸着水の役割

構造最適化および結合エネルギーから，２：１型粘土鉱物の場合，水分子単独で吸着されるケースはほとんどなく，Na^+, Ca^{2+}などの陽イオンを介して吸着されているものと考えられる．仮に水分子が単独で吸着されていたとしても，結合エネルギーが小さすぎて通常の土質試験では感知できない．また，陽イオンを介して吸着する場合，価数が大きいイオンほど水分子を強く吸着するようである．粘着力ｃのメカニズムを論ずる上で，陽イオンの存在とその価数は重要な要素である．なお，計算したモデルには層間陽イオン，層間水が含まれていないが，これらの存在は粘土の電荷を中和する方向に作用するため，各々の結合エネルギーはさらに小さくなる．

３．せん断抵抗角φのメソメカニズム

3.1 真実接触面とφ

せん断抵抗角φのメカニズム解明にあたって対象とした残留強度は，大きなせん断変位を受けてせん断強度が定常値に収束したときの強度で，せん断面は粒子配向により平滑になっている．ゆえに残留状態でのせん断は，平らな面同士の摩擦現象と考えられる．摩擦とは，「接触している二物体が相対的に運動し，または運動し始めるとき，その接触面で運動を妨げようとする向きに力の働く現象，またはその力」[6]と定義され，垂直力に比例することが確認されている（アモントン・クーロンの法則）．摩擦を取り扱う学問・技術分野であるトライボロジーでは，摩擦力が垂直力に比例する理由を次のように説明している．すなわち，物体がある平滑な面で接触しているとき，接触している面は一見すると全面接触しているようにみえる．しかし実際には部分的に接触しているに過ぎず，そのため物体をずらしたときに生じる摩擦力は，この接触部分で発揮される摩擦力の総和となっている．ここで接触部分を「真実接触面（もしくは真実接触点）」といい，真実接触面積が垂直荷重の増加に伴い増えるため全体の摩擦力も大きくなる，である（図６）．せん断現象が摩擦現象であるとすれば，真実接触面が存在し，その面積は垂直力に比例することが予想される．そこで本研究では，真実接触面の存在と垂直力との関係について検討した．なお，メソメカニズムとは，ミクロとマクロを結びつけるメソ（中間）のメカニズムのことで，真実接触面が分子レベルの現象をφというマクロに結びつけている可能性がある．

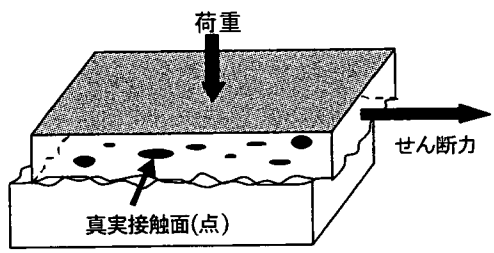

図６　真実接触面の概念図

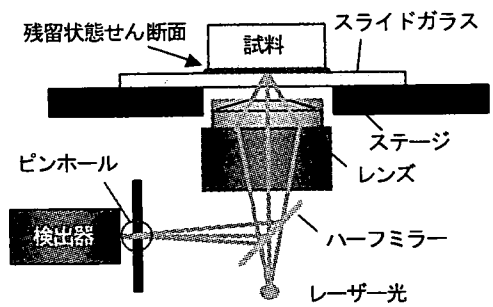

図７　共焦点レーザー顕微鏡による界面観察方法

3.2 試料および実験方法

実験には練り返したＮＳＦ粘土を用いた．残留状態でのせん断面（以後，残留状態せん断面）は，大変位一面せん断試験装置により作製した．せん断箱のサイズは，長さ６０cm，幅３cm，高さ４.５cm と細長く，上せん断箱が可動するタイプである．試験では下せん断箱の端部上面（せん断面部分）に強化ガラス製のスライドガラスを取り付けて，上せん断箱が移動してくると供試体がスライドガラスに載るようにした．試験は圧密定圧条件で行い，垂直応力１５０kPa，せん断変位量２００mm，せん断速度０.５mm/min である．供試体がスライドガラス上に完全に載ったところで供試体をスライドガラスごとせん断箱から外し，両者の接触面を共焦点レーザー顕微鏡（バイオ

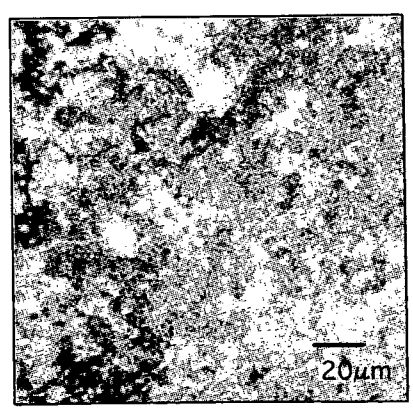

図８　NSF 粘土－スライトガラス界面の共焦点レーザー像

ラッド社，MRC－1024）により下から観察した（図７）．共焦点レーザー顕微鏡（Confocal Laser Scan Microscope, 以後CLSM）とは，レーザーを対象物に照射し，そこから反射した光を検出してコンピュータで画像化する顕微鏡である．特徴は，ピンホールと呼ばれる絞りを利用することで同一焦点（共焦点）面だけの光を検出するため，任意の面の鮮明な光学平面･断面像を得
ることができる．観察にあたりＣＬＳＭの焦点をスライドガラスの上面に合わせ，ガラスと供試体との接触部を観察した．

3.3 実験結果

図８にＣＬＳＭから得られた供試体とスライドガラスの接触部付近の平面像を示す．白色部がガラスと粘土粒子との接触している部分である．図より白色と黒色の明暗の模様が分布していることから両者は部分接触である．図９に加圧試験機により垂直応力を載荷させたときの供試体とスライドガラスとの接触部の平面像を示す．垂直応力をσ_v=0kPa, 24.0kPa, 47.7kPa, 98.4kPaと段階的に増加させるのに伴って全体的に白色が増している様子が認められる．

また，ＣＬＳＭの生画像は黒から白へのグラデーションで表示されるため灰色系の中間色が存在する．接触部分の面積率を算出するにあたり灰色部分を接触部分とするか非接触とするかそのままでは判断が難しいため生画像を全て同じしきい値で白と黒に二値化して総面積における白色域の占める割合を算出した（表２，図１０）．垂直応力の増加に伴って白色域の面積率が増加していることがわかる．白色域の面積増加は，粘土粒子とスライドガラスとの接触面積すなわち真実接触面積の増加を意味する．

3.4 せん断抵抗角φと真実接触面との関係

共焦点レーザー顕微鏡観察より，粘土ーガラス界面は部分接触であり，接触部分の面積，すなわち真実接触面積が垂直力に比例することを確認した．粘土ーガラス界面での検討ではあるが，せん断抵抗角 φ とは，真実接触面が垂直力の増加に伴い大きくなることが，そのメカニズムである可能性が示された．

おわりに

分子軌道法による粘土ー水分子間のエネルギー計算から，２：１型の粘土鉱物であるスメクタイトが陽イオンを介さないと水分子をほとんど吸着しないことが示された．スメクタイトは膨潤性粘土鉱物として知られるが，水の吸着に陽イオンが大きな役割を果たしているようである．

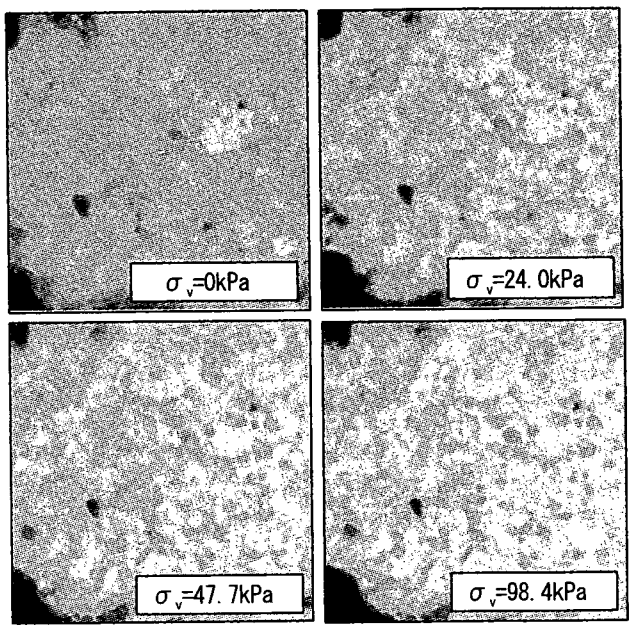

図９　垂直荷重の増加に伴う共焦点レーザー像の変化

表２　白色部分の計測結果

垂直応力 σ_v [kPa]	計測範囲 [μm^2]	白色部総面積 [μm^2]	白色部の占有割合 [%]
0.0	28900	19129	66.19
24.0	28900	21277	73.62
47.7	28900	22803	78.90
98.4	28900	24042	83.19

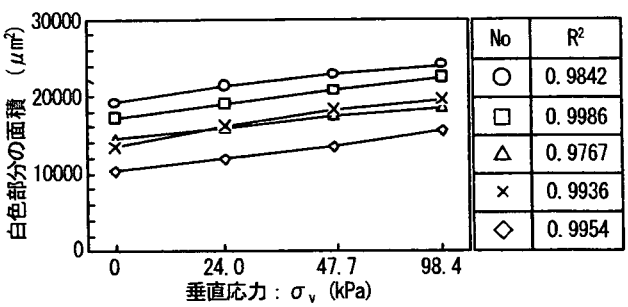

図１０　垂直応力と白色部分の面積との関係

<参考文献>

１）足立格一郎：土質力学，共立出版，296p.,2002.

２）地盤工学会地盤工学用語辞典改訂編集委員会編：地盤工学用語辞典，2006.

３）釜井俊孝：地すべりにおけるすべり面の形成と破壊の伝搬に関する実験的研究，日本大学博士論文，1994.

４）大河原ら：繰り返し一面せん断試験によるカオリン粘土のせん断面の構造と形成過程，地すべり，第37巻，第２号，2000.

５）Grim, R.E.：Clay Mineralogy (2nd ed.)., pp. 51-125. 1968

６）F.P.Bowden and D.Tabor: The Friction and Lubrication of Solids, Oxford, 1954

地盤工学会　北海道支部
技術報告集　第 48 号
平成20年2月　於札幌市

原子間力顕微鏡による異なる温度湿度条件下での高純度粘土の摩擦力･粘性係数

岩手大学大学院　学生会員○久　常　雄大
岩　手　大　学　国際会員　大河原　正文
北海道大学大学院　国際会員　三田地　利之
北海道大学大学院　国際会員　S. B. Tamrakar

1. はじめに

原子間力顕微鏡(Atomic Force Microscope: AFM)とは，探針と呼ばれる極めて小さな針で試料表面を走査することにより，試料表面の形状，摩擦力，粘性，弾性，表面電位，電気力，磁気力などの表面情報を得る顕微鏡である．測定はマイクロメートル～ナノメートルオーダーのミクロ領域を対象とし，真空中，大気中，ガス中，液中など様々な雰囲気中での測定が可能である。

ところで，粘土のせん断強度は，そのほとんどが土粒子集合体である供試体を使って測定されている。そのため得られるせん断強度は，土粒子が有している強度の積分値ともいうべきものである。センチメートルオーダーのデータは膨大にあるものの，供試体を構成する土粒子単体については，対象があまりに小さいため通常の土質試験機では測定できず，強度など地盤工学上の物性値について測定されることはなかった。そこで本研究では，土粒子の粒径程度の大きさを測定範囲として，原子間力顕微鏡による摩擦力（≒せん断力），粘性ならびに表面形状を測定した。あわせて摩擦力，粘性係数の温度依存性についても検証した。なお，本研究での表面形状とは，単に土粒子１個の表面ではなく，一面せん断試験により形成された残留状態せん断面のミクロ表面をさす。せん断面の表面形状は，例えばせん断強度の発現機構を考える上での基礎データとなる。残留状態を対象にしたのは，この状態のせん断面が一般に平滑で，高さレンジの小さいAFMには適しているからである。

2. 試料および供試体作製

試料は，Na-montmorillonite を主成分とするクニピア-F（クニミネ工業），Ca-montmorillonite を主成分とするクニボンド（クニミネ工業），Kaolinite を主成分とするカオリン-KH（カナヤ興産）である。

供試体の作製にあたり摩擦力測定では試料表面が均一で凹凸の小さな試料表面が適するため，粘土懸濁液をシリコンウエハに数滴滴下することで粘土薄膜を作製した。具体的には粘土に蒸留水を加えて1wt.%の粘土懸濁液をつくり，これを超音波洗浄したのち清浄なシリコンウエハに滴下して，室温で乾燥させた。粘性測定では，測定対象物（粘土鉱物）と比較となる基盤（シリコンウエハ）の表面を同時に測定する必要があるためさらに低濃度の粘土懸濁液により粘土薄膜を作製した。具体的には，0.01wt.%の粘土懸濁液をつくりこれをシリコンウエハ上に滴下し，ろ紙を使ってこの懸濁液を吸い取り強制的に乾燥させた。写真１にシリコンウエハ上の摩擦力測定用供試体と粘性測定用供試体を示す。

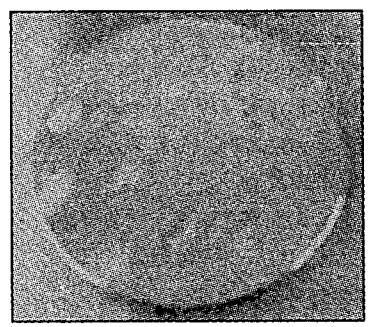

(a) 摩擦力測定用

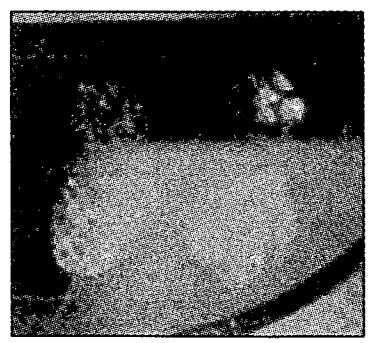

(b) 粘性測定用

写真1　AFM 測定用供試体

3. 測定方法

(1) 摩擦力測定

湿度90%RHと供試体に蒸留水を滴下した状態(湿度100%RH以上)の２条件で，クニピアF，クニボンドおよびカオリンKHの摩擦力を測定した。このとき，ステージの表面温度をそれぞれ 20℃，25℃，30℃，35℃，40℃に設定した。測定条件は，測定範囲５μmの１スキャンライン固定とし，スキャン速度は8.3μm/sec，測定モードはコンタクトモードである。プローブは Cont（ナノワールド社）を使用し凹凸情報を得るたわみと摩擦情報を得るねじれを分離するためにスキャン角度を 90° とした。得られる情報は高さおよび摩擦力である。測定は，試料ステージに取り付けた試料にプローブを近づけてスキャンし，１スキャンライン上で固定した状態でパラメータを調整した後，一定値となった摩擦力を測定した。測定後，フォースモードに移行してフォース･カーブを測定し，垂直力を次式により求めた。ここでFは垂直力(nN)，Kはプローブのバネ定数(N/m)，ΔAはプローブの変位(nm)である。摩擦力を垂直力で割り摩擦係数μを求めた。

$$F = K \cdot \Delta A$$

Measurements of Frictional Force and Coefficient of Viscosity of Pure Clay Minerals under the Different Temperature Conditions using AFM
Takehiro HISATSUNE (Graduate Student, Iwate University), Masafumi OKAWARA (Iwate University), Toshiyuki MITACHI (Graduate School of Engineering, Hokkaido University)

＊温度・湿度制御

試料の表面温度はシリコンラバーヒーターおよび温度コントローラーにより調節した。シリコンラバーヒーターは電気を流すことで発熱するヒーターである。シリコンウエハ基盤の背面にヒーターを接着し温度コントローラーとヒーターを接続した。温度コントローラーに付属する温度センサーで基盤の表面温度を測定し，目的の表面温度になるように温度コントローラーにより制御した。

湿度は，シートで覆った測定室の隙間から加湿器のチューブを差し込み，加湿器の湿度調節つまみを手で回して制御した（写真 2）。

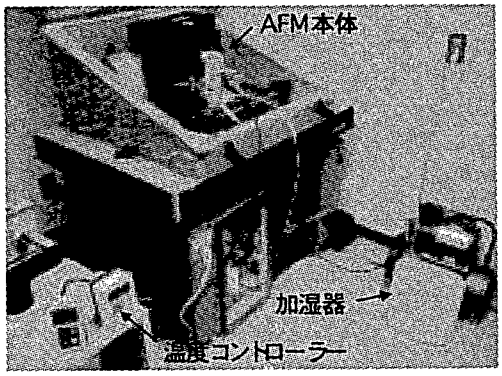

写真2 温度湿度制御した AFM 測定室

(2) 粘性測定

粘性はプローブの位相遅れにより測定される。図 1 は粘性の異なる物質を測定したときの位相差を模式的に表したものである。粘性が高い物質ほど位相が遅れる。

測定に用いた試料はクニピア F，クニボンドおよびカオリン KH である。測定範囲は 10×10 μm，プローブは NCH（ナノワールド社），測定モードはタッピングモードである。測定時のステージの表面温度は 20℃，25℃，30℃，35℃，40℃である。測定手順は，試料ステージに取り付けた試料にプローブを近づけてスキャンを開始し，スキャン開始直後 1 スキャンラインで固定した状態で往復の凹凸波形およびエラー波形が一致するようにパラメータを調整した。調整後，10 μm×10 μm の範囲をスキャンさせ凹凸像および位相像を得た。粘土とシリコンウエハとの位相差は画像解析ソフトにより位相像のコントラストすなわち位相遅れをヒストグラムで表し，ヒストグラムのピーク値を読み取ることにより求めた。

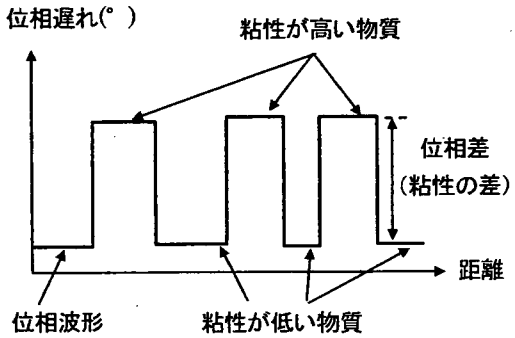

図1 粘性の異なる物質における位相測定

(3) 残留状態せん断面の表面形状測定

大変位一面せん断試験により作製された残留状態せん断面を測定した。比較のためにシリコンウエハに粘土懸濁液を滴下した粘土薄膜の表面形状も測定した。粘土薄膜は，平滑な表面を有するため AFM 測定用試料として使われる。測定は室温，大気中で行い，測定範囲 10×10 μm，プローブは NCH を使用した。測定モードはタッピングモードである。得られた凹凸データをもとに専用の解析ソフトで表面粗さ解析を行った。

4. 実験結果および考察

(1) 摩擦力

図 2 に粘土の表面温度と摩擦係数 μ との関係を示す（摩擦係数 μ＝摩擦力 F／垂直力 P）。垂直力 P はフォース・カーブ測定により算出した。摩擦力 F については使用した AFM に力(nN)に換算する機能がないため，既存の研究[2]において摩擦力が得られているシリコンウエハの表面を測定し，得られた電圧(mV)から換算係数（力／電圧）を求め，測定値（電圧）にこの換算係数を乗じることで摩擦力を算出した。図より粘土粒子の表面温度が 20℃から 40℃へと上昇するのに伴い，90%RH，液中ともに μ は大きくなっている。摩擦係数 μ と温度の回帰直線の r^2 値が 0.95 以上であるから，μ は温度上昇に伴い直線的に大きくなるといえる。また，湿度 90%RH から液中になることで μ が 0.003 から 0.004 と一定の割合で減少した。これは粘土粒子表面に存在する水分が多くなることで粘土粒子の表面で発揮される摩擦力が小さくなったことを示唆している。

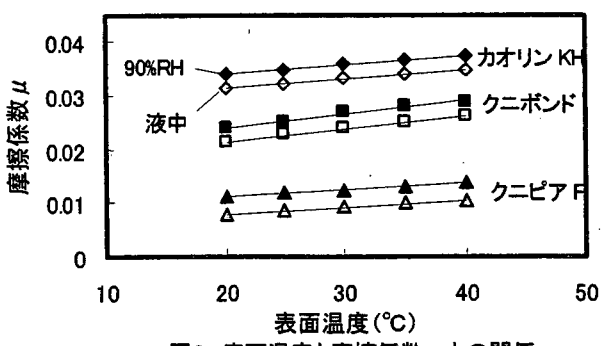

図2 表面温度と摩擦係数 μ との関係

(2) 粘性

図 3 に試料の表面温度と位相差との関係を示す。図から粘土粒子の表面温度が 20℃から 40℃へと上昇するのに伴い，位相差は直

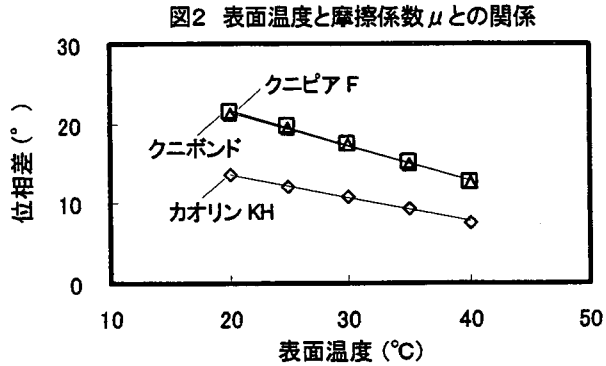

図3 表面温度と粘性との関係

線的に小さくなっている。位相差の低下は粘性の低下を示すことから，温度上昇に伴い粒子表面の粘性が低下したことになる。表1は図3の位相差を平均したものである。表から10℃の温度上昇による位相差の減少はクニピアFとクニボンドで平均4.3°，カオリンKHが平均2.9°であった。スメクタイトを主成分とする膨潤性粘土のほうがカオリン鉱物を主成分とする非膨潤性粘土よりも温度上昇により粘性が低下しやすいことが示唆された。

表1 位相差の平均値

	20℃	25℃	30℃	35℃	40℃
クニピアF	21.2	19.3	17.4	15.0	12.6
クニボンド	21.4	19.6	17.4	15.2	12.6
カオリンKH	13.5	12.0	10.7	9.2	7.6

(3) 表面粗さ

図4にクニピアF，図5にクニボンド，図6にカオリンKHの表面解析結果を示す。図中の(a)は解析範囲の一辺の長さLと算術平均高さRa，(b)は解析範囲の一辺の長さLと表面積増加率RIA，(c)は1周期の凹凸の長さLと高さHである。

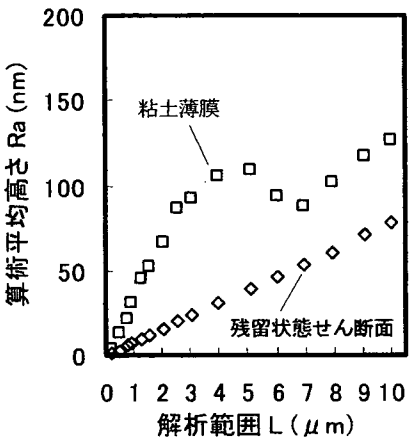

(a) 算術平均高さ Ra

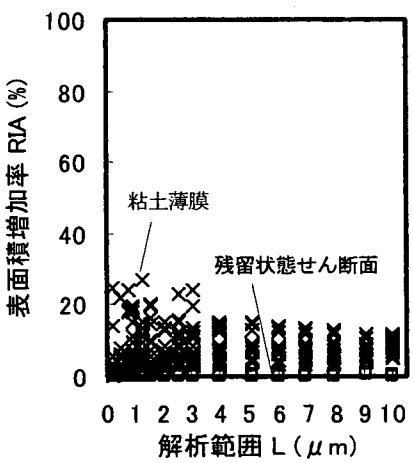

(b) 表面積増加率 RIA

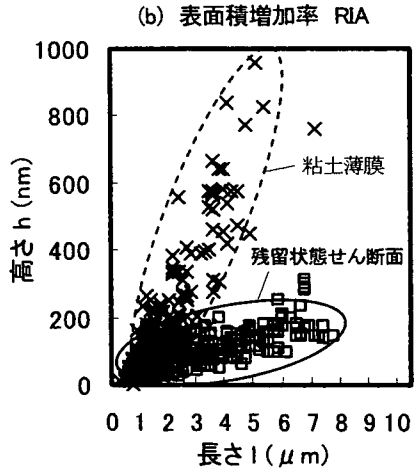

(c) 1周期の凹凸の長さと高さの分布

図4 クニピアFの表面粗さ解析結果

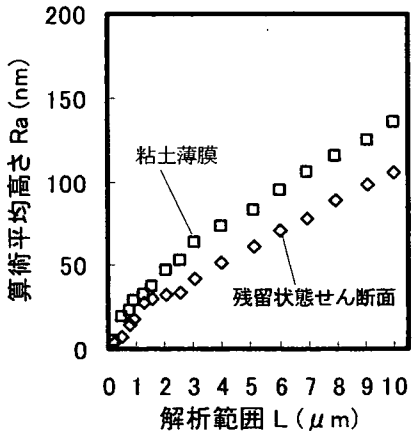

(a) 算術平均高さ Ra

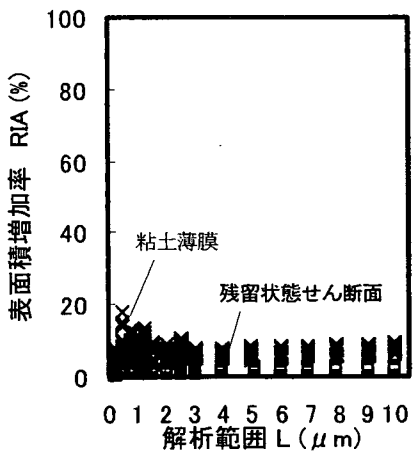

(b) 表面積増加率 RIA

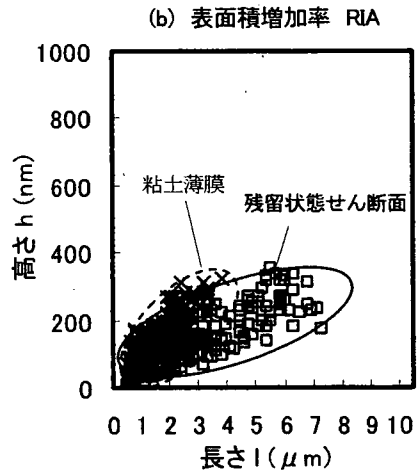

(c) 1周期の凹凸の長さと高さの分布

図5 クニボンドの表面粗さ解析結果

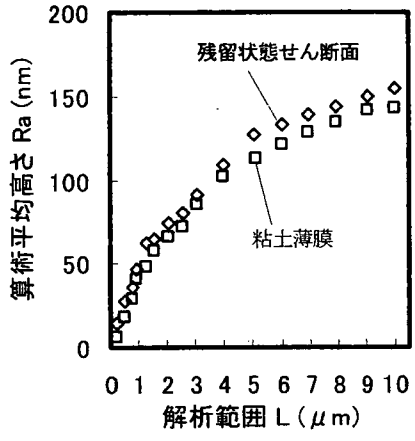

(a) 算術平均高さ Ra

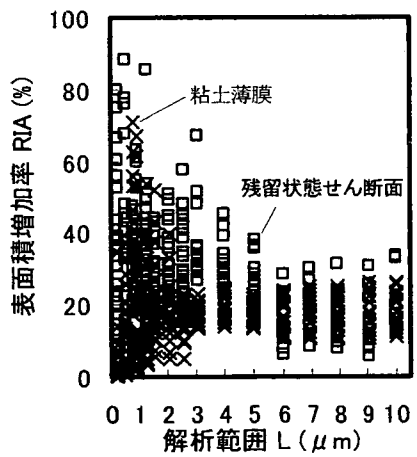

(b) 表面積増加率 RIA

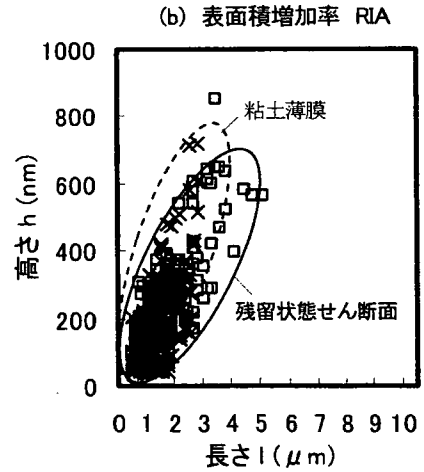

(c) 1周期の凹凸の長さと高さの分布

図6 カオリンKHの表面粗さ解析結果

算術平均高さ Ra は JIS B0601 で定義された表面粗さの代表的なパラメータである。Ra を 2 次元の模式図で示したのが図 7 である。Ra は基準線と粗さ曲線 *f(x)* で囲まれた面積を基準長 *L* で割ったものである。Ra は同じ基準長で基準線と粗さ曲線 *f(x)* とに囲まれた面積が同じであれば，粗さ曲線（凹凸）の形状が異なっても同じ値をとってしまう。表面積増加率 RIA は凹凸の表面積が平面と比較して増加した割合であり，凹凸の大小を示している。そのため仮に Ra が同じでも RIA が大きければ細かい凹凸が卓越し，RIA が小さければ大きな凹凸が卓越することを示す。(c)は 1 周期の凹凸の長さと高さの分布を表したもので，表面の凹凸の大きさを感覚的に捉えるためのグラフである。

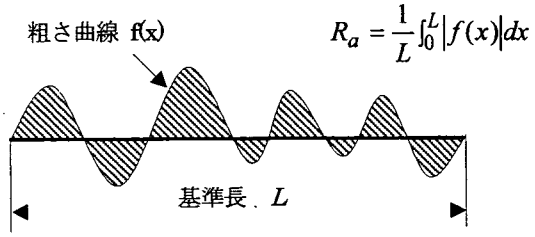

図7 算術平均高さ R_a

まず，図 4(a)，図 5(a)，図 6(a)の算術平均高さ Ra と解析範囲との関係であるが，算術平均高さ Ra の平均値は，クニピア F とクニボンドでは残留状態せん断面よりも粘土薄膜のほうが大きく，カオリン KH はほぼ同じである。Ra の分布状況は，クニピア F の粘土薄膜を除いて解析範囲が大きいほど Ra が大きくなる傾向を示している。クニピア F の粘土薄膜は，解析範囲 5 μm から 7 μm の範囲で Ra が小さくなり，7 μm からまた大きくなる。

次に図 4(b)，図 5(b)，図 6(b)の表面積増加率 RIA について述べる。クニピア F とクニボンドの残留状態せん断面の RIA は解析範囲に関係なくほぼ一定の範囲の値を示した。とくにクニピア F の解析範囲 L=5～7 μm では RIA に変化は認められない（図 4b)。これに対し，カオリン KH の RIA のばらつきは大きい。

図 4(c)，図 5(c)，図 6(c)は，表面凹凸の大きさの分布を視覚的にとらえるための図である。凹凸の長さについてみると，クニピア F とクニボンドの残留状態せん断面は長さ 1 μm から 7 μm の凹凸が存在するが，クニピア F とクニボンドの粘土薄膜とカオリン KH では 4～5 μm 以下の小さい凹凸が多い。凹凸の高さは，クニボンドとカオリン KH はほぼ同じだが，クニピア F は残留状態せん断面よりも粘土薄膜の方が 3～4 倍ほど高い。

クニピア F の場合，残留状態せん断面に比べて粘土薄膜では凹凸の長さが短く，高さが高いことから，Ra が大きくなったと考えられる。クニボンドの場合，残留状態せん断面に比べて粘土薄膜では凹凸の長さが短いため，Ra が大きくなったが，高さはほぼ同じであるためクニピア F ほどの違いは見られない。これに対して，カオリン KH では残留状態せん断面と粘土薄膜で凹凸の長さおよび高さにほとんど差が見られないことから，Ra がほぼ同じ値となった。

以上より，クニピア F とクニボンドの残留状態せん断面は粘土薄膜より平滑で，カオリン KH の残留状態せん断面は粘土薄膜と同程度の平滑さであることが明らかになった。

5. まとめ

AFM により粘土の摩擦力・粘性・表面形状を測定した結果，得られた知見を以下に示す。

① 摩擦係数 μ は，温度上昇（20℃→25℃→30℃→35℃→40℃）に伴い大きくなる。

② 粘性は，温度上昇（20℃→25℃→30℃→35℃→40℃）に伴い小さくなる。

③ 残留状態のせん断面は，粘土薄膜より平滑である。

＜参考文献＞

1) 大河原正文・三田地利之・米田哲朗：第 46 回粘土科学討論講演要旨集,pp.150-151,2002.

2) 山岡武博：フリクショナルカーブによる定量的摩擦特性評価 I ,2001.

Factors affecting tensile strength measurement and Modified Tensile Strength measuring apparatus for soil

Surendra Bahadur Tamrakar[(i)], Toshiyuki Mitachi[(ii)] and Yasuo Toyosawa [(iii)]

i) Research Resident "Rank A", NIOSH, Institute of Industrial Safety, Tokyo, Japan.
ii) Professor, Hokkaido University, Hokkaido, Japan.
iii) Senior Researcher, NIOSH, Institute of Industrial Safety, Tokyo, Japan.

Abstract

In this paper tensile strength measuring apparatus developed by Tamrakar et. al (2005) was used to measure the tensile strength of one dimensionally consolidated saturated NSF-clay and statically compacted unsaturated mixtures of NSF-clay, CFP-silt and Toyoura-sand. Tensile strength (q_t) obtained from the tensile tests were compared with the unconfined compressive strength (q_u). It was observed that the ratio, q_u/q_t lied within the range of 2 to 3 for saturated NSF-clay and 4 to 16 for compacted mixtures. Effect of specimen thickness within the tensile mold, number of compaction layers and tensile pulling rates on the tensile strength were also examined. Comparing the specimen thickness within the tensile mold, it was found that the specimen having 5 cm thickness gave the minimum value. Also, tensile strength increased with the increase in the number of compaction layers. As in other shear strength, increment in the tensile strength was observed beyond tensile pulling rate of 0.34 mm/min. But below this pulling rate also, some increments were observed.

Introduction

Most of the vertical slopes get failed with the development of tensile crack on the top of the slope. Also, many earth dams, embankments, pavements, etc. where soil layers are compacted, are failed due to the development of tensile cracks. Prediction of probable position and depth of tensile crack is necessary to protect the property and loss of lives of workers at the construction site. In order to explain the position and depth of tensile crack, an accurate measurement of tensile strength of soil is necessary. Very few researches (e.g. Suzuki et al., 1998; Yao et al., 2002 and Ono et al., 2003) have been made to measure the tensile strength of soils having lower tensile values. Recently, Nahlawi et. al (2004) and Tamrakar et. al (2005) have introduced new tensile strength measuring apparatus which measures the tensile strength directly. One developed by Nahlawi et. al (2004) could be mainly used for compacted clayey and stiff soils only whereas the one developed by Tamrakar et. al (2005) seems to be easy to use and simple to handle and could be used for both compacted unsaturated and highly saturated soils.

Tamrakar et. al (2005) measured the maximum tensile strength of Kanto loam around 50~60% of water content and showed the ratio of unconfined compression strength and tensile strength around 12.5 which varied with the water content. They also showed the effect of amount of finer particles and their size on tensile strength. Possible measurement of tensile strength for saturated NSF clay was also shown.

In this paper, tensile apparatus (type-A tensile mold) developed by Tamrakar et. al (2005) was used to measure the tensile strength of saturated and unsaturated soils. Also, the effect of number of compaction layers, thickness of the specimens and tensile pulling rate on the tensile strength was studied. Unconfined compression tests were also performed to compare their values with tensile strength.

Test Apparatus

Tensile test apparatus shown in Photo 1 consists of horizontal platform upon which apparatus box having two halves; fixed box and movable box, is placed. Inside this box, two tensile molds are

placed. The inner shape of this mold is like "C" structure and it holds the specimen. Two molds are screwed to the apparatus boxes separately. One box of the apparatus is fixed to the horizontal platform while the other box can move freely on the horizontal platform. To reduce the friction, linear sliding roller is placed between the movable box and platform. Movable box is pulled away in horizontal direction until the soil specimen fails in tension with tensile crack appearing at the middle of the specimen where two halves of the mold is attached. Load cell placed between the movable box and motor axis measures the tensile load. This tensile load divided by the area of the tensile crack perpendicular to horizontal pulling direction, gives the tensile stress. These molds can be easily changed as they are connected to the main apparatus by the screws only. The total surface area of this mold is 38.5 cm^2. The minimum width at the constricted section of this mold is 3 cm and the depth is 5 cm.

The apparatus box along with the mold and platform can be completely separated from the motor for preparing the specimen before the test. Compacted soil specimen is prepared within this mold by direct static compression. Once the specimen is ready within the mold for the test, then it is connected to motor shaft. Between the motor shaft and movable apparatus box, there are some attachments where load cell is kept.

Photo 1. New tensile strength measuring apparatus (inset : tensile molds) (Tamrakar et. at (2005).

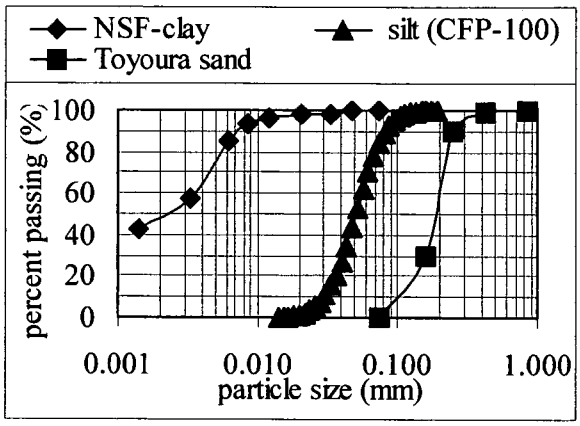

Fig. 1. Grain size distribution curves.

Materials and Specimen Preparation

Kanto loam, NSF-clay and the mixtures of NSF-clay, CFP-silt and Toyoura-sand were taken as test materials. NSF-clay is commercially available clay which consists of Pyrophylite, CFP-silt (100) is crushed form of Silica sand and Toyoura-sand is also commercially available standard Japanese sand. Grain size distribution curves and index properties for these soils are shown in Fig. 1 and Table 1. Now onwards, NSF-clay, CFP-silt and Toyoura-sand are represented by clay, silt and sand, respectively. For saturated test specimen, consolidated clay specimens were used where as mixtures of clay, silt and sand in different proportions were used for unsaturated compacted specimens. Table 2 and 3 show the proportions and test conditions for different mixtures.

Before preparing the specimens, at first, tensile molds were fixed into the apparatus box and screwing was done between the movable box and apparatus horizontal plate so that movable box would be fixed. To reduce the friction between the specimen and the inner wall of the tensile mold, thin film of grease was applied over its inner surfaces. After the insertion of the consolidated specimen in case of saturated specimens or after the completion of compaction in case of compacted specimens into the tensile mold, load cell is set up towards the pulling side of mold box. Finally, the screws which are earlier fixed to prevent the movement of movable box of the apparatus are un-screwed

Table 1 Properties of test materials

Materials	density	dry density		w_L	w_P
	soil solid	max.	min.		
	g/cm^3	g/cm^3	g/cm^3	(%)	(%)
NSF-clay	2.78			55.1	30.6
silt (CFP-100)	2.66	1.59	1.17		
Toyoura sand	2.64	1.65	1.34		

Saturated specimens were prepared by pre-consolidating the slurry of the clay material in a separate, special consolidation mold. Two-way drainage with one dimensional consolidation was done. Once the consolidation was over, consolidation mold with consolidated specimen was placed over the tensile mold. Centering of molds was done by guiding support screws which were attached to the fixed portion of the apparatus box. By pushing the shaft of the consolidation mold slowly, consolidated specimen was allowed to insert into the tensile mold. Once the full depth (5 cm) insertion was completed, then the specimen was cut and its upper surface was trimmed.

Table 2 Test mateials for mixtures of clay, silt and sand.

dry density	NSF-clay	CFP-silt	Toyoura-sand	q_u	q_t	q_u/q_t
(g/cm^3)	%	%	%	(kPa)	(kPa)	
1.50	25	-	75	21.1	3.2	6.5
	40	-	60	55.9	6.6	8.4
	50	-	50	74.4	7.8	9.5
	60	-	40	79.1	8.6	9.2
	75	-	25	131.3	12.1	10.9
1.50	25	75	-	64.3	6.9	9.3
	40	60	-	100.0	8.4	11.9
	50	50	-	97.8	8.5	11.5
	60	40	-	132.2	10.3	12.9
	75	25	-	182.2	11.7	15.5
1.40	-	25	75	6.6	1.4	4.6
	-	40	60	12.9	2.2	6.0
	-	50	50	16.4	2.7	6.1
	-	60	40	18.7	3.0	6.2
	-	70	30	26.7	3.9	6.9

In case of compacted specimens, at first, materials were thoroughly mixed with required distilled water and kept in an air tight plastic bag and sealed so that water was uniformly distributed throughout the materials. Specimens were prepared either under constant stress or under constant dry density conditions. In both the conditions, compacted specimens were prepared by directly and statically compressing the prerequisite amount of soil kept within the tensile mold of the apparatus, using bellophragm cylinder. Collar was generally placed over the tensile mold to prevent falling out of soil from the mold. Specimens were compacted keeping the dry density, water content and thickness of the specimens constant. Thickness, number of compaction layers and tensile pulling rates were varied depending upon the test conditions.

Table 3 Mixing propertions and Testing conditions for clay ~ sand mixtures.

Specimens	Mixing ratio	w	Controlled			Testing Conditions
			dry density	compaction stress	dry density	
	(by wt.)	(%)	(g/cm^3)	kPa	(g/cm^3)	
clay~sand	3:1	10.0	1.50			No. of layers[(1)]
clay~sand	3:1	10.0	1.50			Thickness[(2)]
clay~sand	1:3	10.0		200	1.54	Pulling rate[(a)]
clay~sand	3:1	10.0		200	1.26	
clay~sand	3:1	10.0	1.50			Pulling rate[(b)]
clay~sand	1:3	10.0	1.50			

[(1)] one, two and four layer-compaction, [(2)] 1.25, 2.5, 3.75 and 5 cm

[(a)] 0.01, 0.09 and 0.34 and 0.88 mm/min, [(b)] 0.17, 0.34 and 0.88 mm/min

In case of unconfined compression test, saturated specimens were prepared by pre-consolidating the clay specimens in an ordinary consolidometer where as unsaturated compacted specimens were prepared in a normal splitting mold either under constant stress or constant dry density condition. Generally, one layer compaction was done. But to see the effect of numbers of layer of compaction, some specimens were prepared with one, two, three, four, five and ten layers.

Test Conditions

Tests in which specimen thickness was maintained at 5 cm with one-layer compaction and pulled under 0.34 mm/min tensile pulling rate, were considered as Reference tests. All the tests of saturated specimens are reference tests. Saturated specimens of clay were prepared under 100, 200 and 300 kPa. Water content, density, degree of saturation, etc. is shown in Table 4.

In case of unsaturated specimens, test conditions were changed depending upon the type of tests. Mixtures of clay, silt and sand specimens were prepared by mixing them in different proportions as shown in Tables 3 and 4. Specimens were compacted keeping their dry density, water content and specimen thickness constant. In case of tests where the effect of specimen thickness was studied, specimens were prepared by one-layer static compaction and they were pulled with 0.34 mm/min. In this case specimen thickness varied from 1.25 to 5 cm. Similarly, where the effect of number of layers of compaction was studied, specimens were prepared with one-layer, two-layers, three-layers and four-layers of static compactions, keeping the overall specimen thickness to be around 5 cm and pulling them under 0.34 mm/min. In case of the tests where the effect of tensile pulling rate was studied, specimens were prepared by one-layer static compaction with specimen thickness of 5 cm. In this case, tensile pulling rate was varied from 0.09 to 1.75 mm/min.

ble 4 Saturated sol specimens conditions and test resu

Specimen type	NSF-clay				
Preconsolidation pressure	100	200	200	300	300
Soil unit weight	27.23	27.23	27.23	27.23	27.23
Water content w (%)	55.51	45.03	46.65	45.61	42.84
Degree of saturation S_r (%)*	98.40	97.20	96.70	98.75	96.00
q_t (kPa)	13.54	18.34	20.64	25.35	27.04
q_u (kPa)	29.81	52.81	52.81	77.12	77.12
q_u/q_t	2.20	2.88	2.56	3.04	2.85

* for tensile test

Unconfined compression test for saturated specimens were prepared by trimming the pre-consolidated specimens whereas unsaturated compacted specimens were prepared using ordinary splitting mold. Other than those for the effect of number of compacted layers, all the compacted specimens were prepared by one-layer static compaction using bellophragm cylinder. Other conditions such as dry density and water content were kept same as those for tensile compacted specimens. Compacted layers were prepared with 1, 2, 3, 4, 5 and 10 layers. Compaction time allowed for each layer was around 1 minute. The height and depth of specimen for both saturated and unsaturated cases were 10 cm and 5 cm, respectively. Unconfined compression tests were conducted at constant displacement rate of 0.1 mm/min.

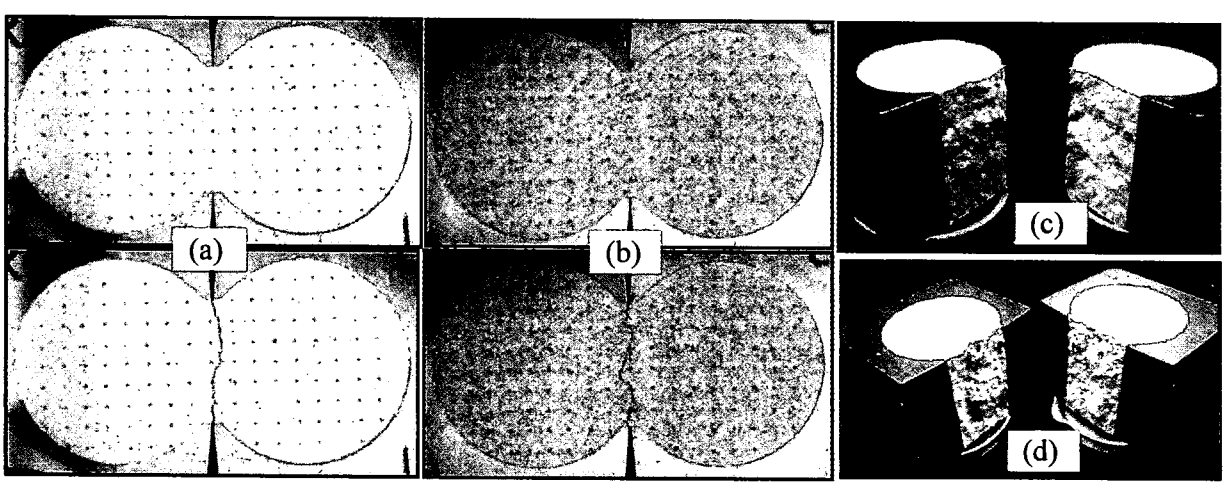

Photo 2 Photographs before and after the tensile failure. (a) and (c) clay ~ sand mixture (3:1) and (b) and (d) clay ~ sand mixture (1:3).

Results and Discussions

Photos 2(a) and (b) showed the photographs before and after the tensile failure tests for clay~sand (3:1) and clay~sand (1:3), respectively. Clear and straight tensile crack (failure line) could be seen. In Photos 2(c) and (d), failure planes (tensile crack plane) after the tests were shown. Clear and smooth failure surfaces could be seen.

Tensile stress ~ displacement curves obtained for the saturated specimens of clay (pre-consolidated under 100, 200 and 300 kPa) are shown in Fig. 2. As shown, with the increase in consolidation pressure, there is increase in tensile strength. Small variation in the test result might have occurred either during the transferring of the consolidated specimen from the pre-consolidometer to tensile mold or during the trimming of the specimen surface. In addition, variation in the water content (degree of saturation) or the friction between the inner wall of the consolidation mold and slurry material during the pre-consolidation might also have affected small change in their strength. Henceforth, proper attention must be paid during the specimen preparation. Stress ~ displacement curves for clay~silt~sand (1:1:1) obtained from tensile test and unconfined compression tests were shown in Figs. 3(a) and (b), respectively. Clear peak for tensile stress as well as unconfined compressive stress could be seen. Here, tensile stress measured was shown in negative value. From now onwards, tensile strength values would be shown as positive values.

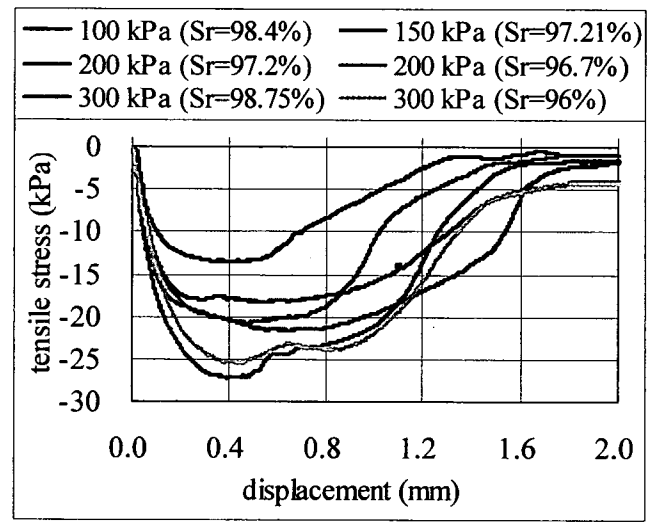

Fig. 2. Tensile stress ~ displacement curves for consolidated NSF-clay.

In Table 4 shows the tensile strength and unconfined compression strengths obtained for saturated specimens. Increase in both tensile and unconfined compression strengths with the increase in the consolidation pressure could be seen. It was observed that the ratio of q_u/q_t for saturated clay varied from 2~3. Another type of NSF-clay used by Tamrakar et al. (2005) had shown the average ratio as 6. All the test specimens shown in Table 4 have more than 93% of degree of saturation. Degree of saturation (S_r) shown in the Table 4 was calculated by using unit wet of soil solid, total weight of the specimen inside the tensile mold and the water content of the specimen after failure. As it is difficult to measure the area of the specimen directly, the total area of the specimen was considered to be same as that of the tensile mold. Thickness of the specimen was measured once the trimming was done after transferring the consolidated specimen into the tensile mold. It was assumed that the specimen tightly fits into the mold. Ratio of q_u and q_t for clay~silt~sand (1:1:1) specimen was found to be 8.6. In Tables 2 and 3, tensile and unconfined compression strengths measured for different mixtures are shown. It could be seen that the ratio of q_u/q_t for the unsaturated mixtures varied from 4 to 16. Tamrakar et al. (2005) had also measured the similar ratio of q_u/q_t for Kanto loam which varied from 10 to 13 (Tamrakar et al., 2005).

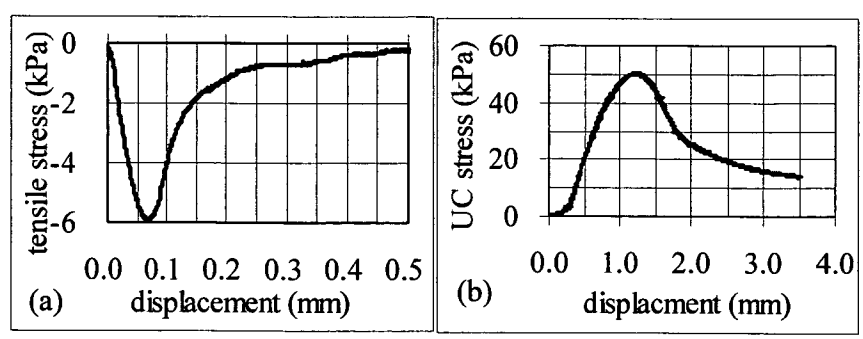

Fig. 3. Stress ~ displacement curves for clay ~silt~sand (1:1:1) mixture (a) tensile test and (b) unconfined compression test.

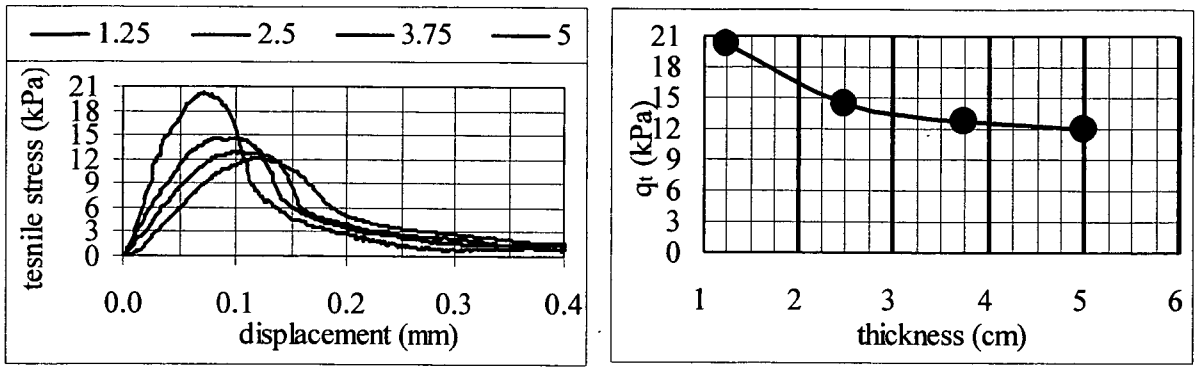

Fig. 4 Effect of thickness on q_t (a) Stress ~ displacement curves and (b) tensile strength.

Effects of specimen thickness are shown in Figs. 4. Here, tensile strength values for different specimen thicknesses are shown. Decrease in the tensile strength with the increase in the specimen thickness could be seen. Specimen having 5 cm thickness, i.e., the thickness of tensile mold, showed the minimum tensile strength. Here, specimens were compacted only once for all the thicknesses. Therefore, uniformity in the density is more in case of specimen which had the minimum thickness. Irrespective of specimen thickness, tensile pulling for each test was done from the mid-height of the tensile mold. With the change in the thickness, resultant pulling direction might have changed, hence affecting the strength.

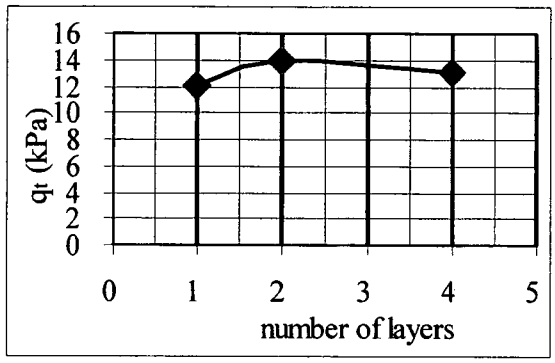

Fig. 5. Effect of number of compaction layers on qt for clay ~ sand mixture (3:1).

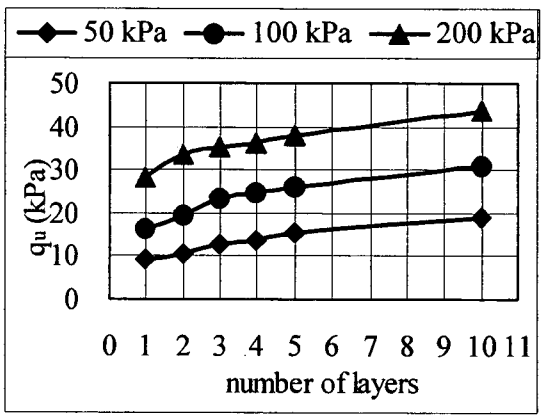

Fig. 6. Unconfined compression test results for clay ~ sand mixture (3:1).

The effect of number of layers of compaction to tensile strength is shown in Fig. 5. During this test, 5 cm thick specimens were prepared by compacting predetermined amount of specimen within the tensile mold in one-layer, two-layer, three-layer and four-layer. Clay-sand mixture (3:1, w=10% and rd=1.5 g/cm3) showed the increment in tensile strength with the increase in the number of compaction layers. One-layer compaction gave the minimum value than those obtained for two, three and four-layer compaction. With the increase in number of compaction layers, more uniformity of density through out the specimen takes place and this will increase the strength of the specimen. Similar test result was seen in case of unconfined compression test shown in Fig. 6 where test specimens were prepared by statically compacting the same amount of clay-sand mixture (1:3, w~10%, compaction pressure 50, 100 and 200 kPa) with 1, 2, 3, 4, 5 and 10 layers. As shown in Fig. 6, at the beginning, sudden increase in q_u strength was seen but the rate of increment decreased with the increase in the number of layers. As obvious, with the increase in number of layers of compaction, more uniformly dense specimens were obtained which makes the bonding between the soil particles more strong and hence, strength is increased.

Figure 7 shows the tensile strength test results of different soils conducted at different pulling rates which varied from 0.01 to 1.75 mm/min. In Fig. 7(a) clay-sand mixtures (1:3 and 3:1) prepared under 200 kPa were shown where as in Fig. 7(b) same soil specimens prepared under constant dry unit were shown. Comparing the tensile strength of each specimen with respect to tensile pulling rate, variation in the strength with the change in the pulling rate could be observed

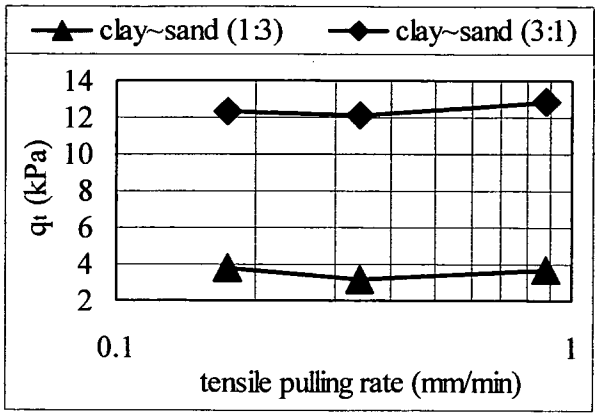

Fig. 7(a). Effect of tensile pulling rate on tensile strength (under controlled pressure).

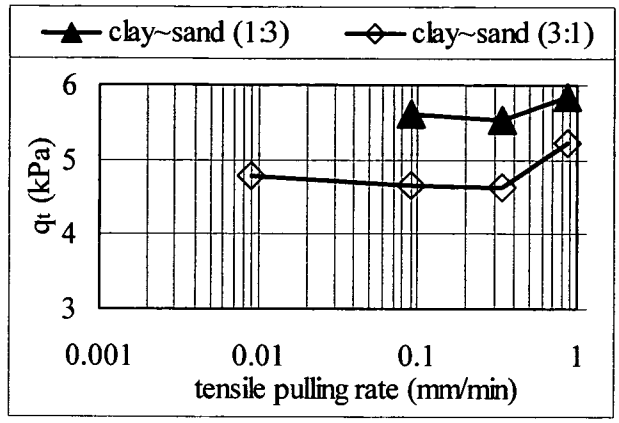

Fig. 7(b). Effect of tensile pulling rate on tensile strength (under controlled dry density).

for all types of soil specimens. It was observed that the tensile strength measured in the range of 0.1 to 0.34 mm/min pulling rate gave the minimum value. In contrary to this, tensile strength measured at the higher and lower tensile pulling rates than 0.1 mm/min showed larger values. This difference in the tensile strength might have occurred while pulling the specimens where soil particles are attached to each other either by suction or internal bonding or cohesion. Tamrakar et al. (2005) had discussed about the relationship between the tensile strength and suction to some extent. Effect of suction at higher and lower tensile pulling rates are yet to be studied. Increment in the tensile strength at higher tensile pulling rate is obvious as in any other shear strength. One reason for the increment at very low pulling rates might be due the dryness on the surface of the specimen as it takes very long time. Other reasons are yet to study.

Conclusions

From the tests conducted for saturated and statically compacted unsaturated soils, following points could be concluded;

1. Stress-displacement curves obtained for both saturated and compacted unsaturated specimens show the possibility of measuring tensile strength with the apparatus used here.

2. Ratio of unconfined compression strength and tensile strength (qu/qt) for NSF-clay was found to be 2~3. For unsaturated soils this ratio varied from 4 to 16 depending upon the type and water content of the soil.

3. From the test results of clay-sand mixture (3:1), it was found that 5 cm thick specimen gave the minimum tensile strength in comparison to other specimens having thickness smaller than 5 cm. Therefore, it is recommended to pull the specimen from its mid-height.

4. Effect of number of layers of compaction (one-layer, two-layer and four-layer) on tensile strength was also studied. It was found that with the increase in the number of compaction layers, there was increase in tensile strength. Similar result was obtained in case of unconfined compression test also. Increment in the strength might have occurred due to increase the uniformity of density distribution throughout the specimen.

5. Effect of tensile pulling rate for variety of unsaturated soil specimens was carried out. It was found that with the increase in the tensile pulling rate beyond 0.34 m/min, tensile strength also increases. But below this pulling rate also, some increments were observed.

Acknowledgements

This research is partially carried out under the Health and Labor Sciences Research Grants of Ministry of Health, Labor and Welfare, Japan.

References

Nahlawi, H., Chakrabarti, S. and Kodikara, J., 2004, "A direct tensile strength testing method for unsaturated geomaterials," Geotechnical Testing Journal, Vol. 27, No. 4, pp. 356–361.

Ono, N., Mochizuki, A., Kurosaki, H. and Ueno, K., 2003, "Trial tests with compressive and tensile strength measuring apparatus," 58th Annual meeting of Japanese Society of Civil Engineers, pp. 337–338 (in Japanese).

Suzuki, T., Umei, T. and Sunaga, F., 1998, "A research on the tensile strength of cement treated soils," 53rd Annual meeting of Japanese Society of Civil Engineers, pp. 600–601 (Japanese).
Tamrakar, S.B., Toyosawa, Y., Mitachi, T. and Itoh, K., 2005, "Tensile strength of compacted and saturated soils using newly developed tensile strength measuring apparatus," Soils and Foundations, Vol. 45, No. 6, pp.103-111.

Tamrakar, S.B., Mitachi, T., Toyosawa, Y. and Itoh, K., 2005, "Development of a New Soil Tensile Strength Test Apparatus," Geo-Frontiers 2005, GSP 138 Site Characterization and Modeling, ASCE.

Yao, S., Masui, T. and Ito, A., 2002, "The relationship between tensile strength and the state of water in Kaolin clay," 47th symposium on Geotechnical symposium, pp. 127–132 (in Japanese).

International Geotechnical Symposium "GEOTECHNICAL ENGINEERING FOR DISASTER PREVENTION & REDUCTION"
July 25-27, 2007
Yuzhno-Sakhalinsk, Russia

Possible use of Tilt-sensor for failure movement and failure plane just before slope failure

S. B. Tamrakar[1], Y. Toyosawa[1], T. Mitachi[2], K. Itoh[1], K. Takashi[3]

[1]Construction Safety Research Group, Japan National Institute of Occupational Safety and Health, Tokyo, Japan
[2]Graduate School of Engineering, Hokkaido University, Hokkaido, Japan
[3]Akebono Brake Industry Co. Ltd., Saitama, Japan

Abstract

In reference to SSC type tilt sensor (Tamrakar et. al, 2005), SL type tilt sensor was designed here by placing three sets SSC type of tilt sensor, separately on each attachment table which are jointed to one single, straight and long flexible plastic plate. Depending upon the position of SSC on SL, they are called as SLU (uppermost), SLM (middle) and SLL (lowermost). As SL type tilt sensors are inserted into slope during excavation, they could measure not only the movement of upper layer of the slope but also inner layers. Applicability of SL sensor was tested in the laboratory by conducting a small scale full size test (60 degree angle) with River sand. Manual excavation around the lower part of the slope was continued till failure occurred. Sharp increment in the tilt angle just before the failure could be observed for each set of tilt sensor inserted on slope surface and slope top.

Keywords: *tilt sensor, failure, slope movement, small scale full size test.*

1 Introduction

Measurement of the displacement and deformations of ground surfaces are generally carried out at the construction sites where embankment or excavation and reclamation works are carried out. Most of the measurements are made to find the amount of settlement or movement along vertical and horizontal directions. But in case of construction works where excavation of slope is made either for retaining wall construction or for the stability of slopes, sometimes movement of slope takes place all of sudden taking the live of workers and damaging the property around the site. To prevent the accident, constant observation of slopes is important. But in general at the beginning movements are very small which is difficult to distinguish by naked eyes and just before the failure, movement becomes fast which makes no time to workers for the escape. Many researches have been presented various methods of measuring the movement of the slope. Most of them are either difficult of set up or expensive of to use in wide working field. Recently, Tamarkar et. el (2006) have developed small size compact type (SSC) and stand alone (SA) type tilt sensors which could be used in the field. These sensors could measure the movement of slope during and just before the failure. But SSC type tilt sensors are generally placed on the slope surface and slope top only. They could measure only the movement of top surface of the slope. During the slope failure, some kind of failure plane is generally seen where upper layer of slope slides over the sliding plane over the lower layer. It would be better if failure plane could be predicted in advance.

In this paper, possibility of measurement of movement of inner layers of the slope including the upper layer was tried using the SSC type tilt sensors during and just before the slope was tried. This was done by conducting small size full scale test within the laboratory so that it could be applied in the real excavating field in the future.

2 Tilt sensors

Tilt sensor used here consists of either one or two sets of highly sensitive accelerometer (Fig. 1(a)). Highly sensitive accelerometer is light in weight and small in size (9x5x11mm). It is made of three silicon layers; outer two layers act as fixed electrodes and inner middle one layer acts as movable electrode as shown in Fig. 1(b). When the accelerometer position is changed (tilted), this movable electrode moves so that distance between the fixed and movable electrode changes. With the change in distance between the electrodes, output capacitance changes and it further changes the output voltage. By calibrating this output voltage with the change in tilt angle, one can measure the tilting angle. The sensitivity of accelerometer used here is 100mV/deg with ±20° measurement range. Thermal sensitivity is around 10 mV/°C. General outline of the tilt sensor is shown in Fig. 1(c) (Tamrakar et al,.2006). This is a small size compact type (SSC) tilt sensor in which two sets of accelerometers were placed in such a way that it could measure both ± tilt angles along X and Y direction. These are placed above the base plate which is supported by the tubular hollow pipe cut into an

angular shape so that it can be easily inserted into the soil without propagating the crack (with less disturbance). SSC type tilt sensors are directly inserted into the slope (as well as slope top). In this case, top portion of the sensor lies well above the slope ground. With this sensor, tilt angle of the outer layer of the slope could only be measured.

In this research, as the movement of inner layers of the slope are tried to measure. Therefore, SSC type tilt sensor is little modified. Only the top portion of SSC type tilt sensor which consists of two accelerometers is used. These are attached to a flexible and thin acryl plate with the help of small attachment tables. In this paper, this type of tilt sensor is named as SL type tilt sensor and depending upon the positions of table on the acryl plate, each group of sensor are termed as SLU (for the uppermost), SLM (for the middle) and SLL (for the lowermost). Here, in one model test, two attachments are only made (only SLU and SLL) where as in another test three attachments are made (SLU, SLM and SLL). Distance between SLU and SLM is 15 cm. Therefore, SLU and SLL are 30 cm apart. In Fig. 1(d), SL type tilt sensor with three sets of sensors is shown. In the experiment here, both SSC type and SL type tilt sensors were used so that comparison between could be made.

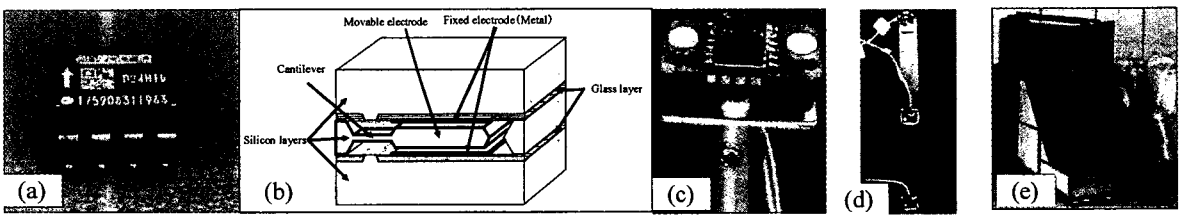

Figure 1. (a) Model test

3 Small Size Full Scale Test

To test the applicability of SL type tilt sensor during the excavation of lower portion of the slope, a small size full scale test was done in the laboratory using a test box shown in Fig 1(e).

3.1 Test Box and Model Slope

To make the model slopes within the laboratory, test box made up of wooden planks shown in Fig. 1(e) was used. This test box has two sections; lower (1.35mx 2.7m x 1.32m) and upper (1.35m x 1.2m x 0.88m). These sections facilitate in modeling the slopes with different slope heights and slope angles. At the beginning, model box is surrounded from all the sides by the wooden planks except the upper face. River sand mixed with water (around 8%) was poured into the text box. Then leveling and compaction were done manually in layers. These processes are repeated until both the sections were filled up. To cut the fill up into desired slope, wooden planks from the front and side walls were removed carefully. Slope of desired angle and height was then made by trimming. Here, thickness at the bottom was kept around 30cm so that trench excavation is possible. Two types of slope made are in Figs. 2(a) and 2(b) for shorter height (SH) and longer height (LH), respectively. At first, SH slope was made and once it was failed, then LH slope was made behind it. Properties of the model slopes are shown in Table 1. Water content and bulk density along the depth of the model slopes measured were varied to some extent.

Table 1. Properties of model tests.

Slope type	Shorter height (SH)	Longer height (LH)
Water content (%)	7.18~8.38	7.00~8.00
Bulk density, ρ_t (g/cm^3)	1.59~1.66	1.59~1.66
Slope angle (°)	60	60
Slope height (cm)	98.00	190.50
Back fill	Yes	No
No. of cuts	10	13
Total failure time (minute)	70.50	94.50

3.2 Instrumentation Set Up and Excavations

In order to measure the movement of the slope surface and slope top, two types of tilt sensors (SSC and SL types) mentioned above were used along with the laser sensors. SL type tilt sensors (SL1, SL2 and SL3) are used to measure the tilt angles of upper and inner layers where as SSC type tilt sensors (SSC1, SSC2 and SSC3) are used to measure the tilt angle of upper layer of slope only. To set up the SL type tilt sensor, at first, long hole was drilled at the desired position with less than 30cm depth and then the SL tilt sensor was inserted into that hole as shown in Fig. 2(c) and 2(d). Spaces between the SLL and SLM, and SLM and SLU are filled up by sand. Slight tamping and compaction was done. Insertion is stopped when SLU just lies on the slope level. In case of SSC, tubular pipe attached to its base is inserted on to the slope ground so that its accelerometers lie well above the ground level. Approximate position of each sensor is shown in Fig. 3. Schematic diagrams for these tilt sensors are shown in Figs. 4(a) and 4(b). Laser sensors are used to measure the movement of the slope surface (S1, S2 and S3) and deformations of slope top. In case of slope top, vertical

displacement is measured by V1 and V2 laser sensors and horizontal displacements by H1 and H2 laser sensors. In Figs. 3(a) and 3(b), set up position for each sensor in each type of test are shown.

After the set up of instruments, manual excavations were started from the lower portion of the slope manually, starting the excavation from the center and moving away from the center towards left and right sides of the slope. Both toe and trench excavations were made. Sequences of excavation carried out were shown in Figs. 4(c) and 4(d) where each step was represented by numbers; 1, 2, 3, 4, etc. In both the slopes, at first toe excavations were carried out and which was later on followed by trench excavations. Width of each toe excavation was about 5.5cm and the depth of each trench was maintained at 10cm except for 10^{th} cut of SH slope and 13^{th} cut of LH slope. About 5 minutes of waiting time was allowed between each excavation to see the movement of the slopes (both slope and top) after the excavation. Excavation was continued until failure of slope took place. For SH slope, under-cutting was done at the 10^{th} cut. Similarly, for LH slope, trimming of excavated surface was done at 13^{th} cut.

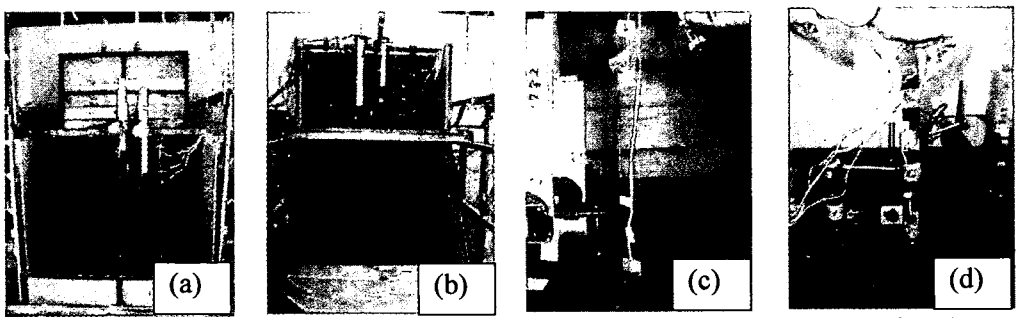

Figure 2. (a) SH model slope, (b) LH model slope, (c) SL set up for SH slope and (d) SL set up of LH slope.

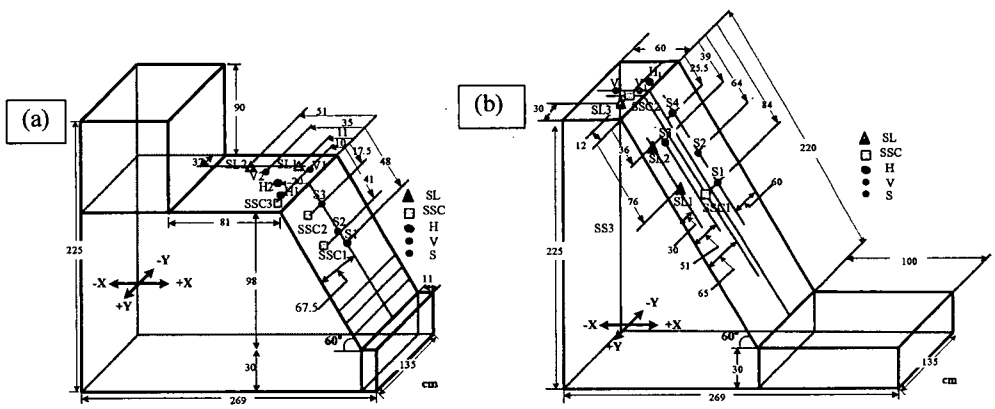

Figure 3. Positions of SL, SSC and laser sensors (a) SH type slope and (b) LH type slope.

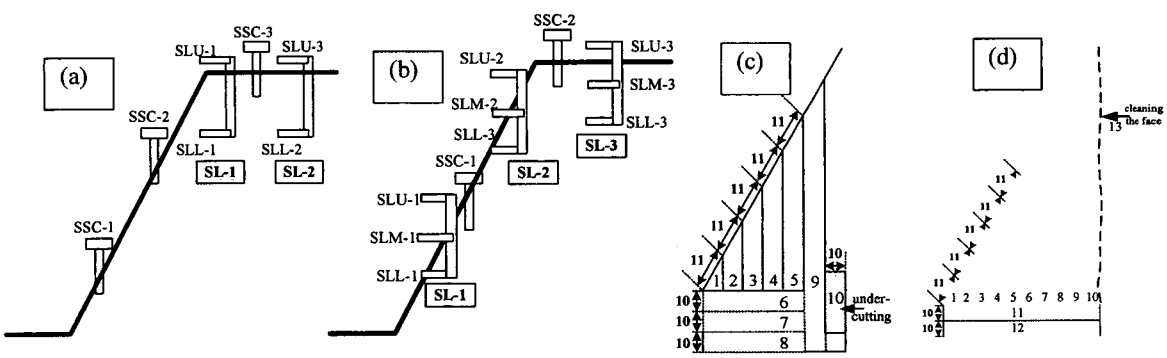

Figure 4. SL and SSC type tilt sensors for (a) SH slope, (b) LH slope and excavation steps for (c) SH slope and (d) LH slope.

4 Test Results and Discussions

In Figs. 5(a) and 5(b), slopes after failure are shown. Failure within the slope was seen in case of SH slope, especially towards the right side of the slope while carrying out the under-cutting of the slope toe at 10^{th} cut. Failure was seen after 70 minutes. Failure

within the slope as well as toward the right side of the slope might have occurred due to small variation in the water content and unit weight within the model slope. In case of LH slope, failure was occurred while trimming the excavated wall of the slope at 13th cut. Failure of the slope was seen after 94.5 minutes. In contrary to SH slope, failure of whole slope was observed in this case except a small portion at the top right corner which might be due to the variation in water content and unit weight within the slope. Here, failure was extended in the slope top also; about 12 cm width from the crest of the slope. Therefore, LH showed deeper depth of failure area than SH slope. Comparing the two slopes, it showed that SH slope was failed when more than 87% of its slope length (surface) was excavated along with the trench. But SL slope was failed when 50% of its slope length was excavated along with the trench. This shows that the with increase in the slope length (slope height), the possible width of toe excavation decreases which is obviously due to the pressure behind the cut that increases with the slope length.

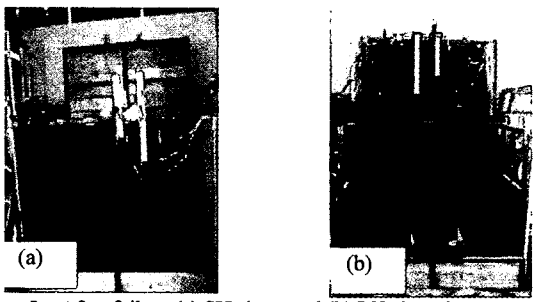

Figure 5. After failure (a) SH slope and (b) LH slope laser sensors.

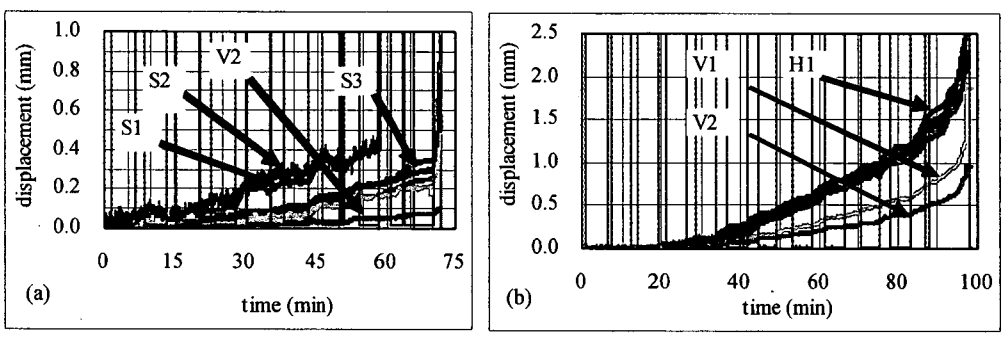

Figure 6. After failure (a) SH slope, (b) LH slope and laser sensors measurement (c) SH slope and (d) LH slope.

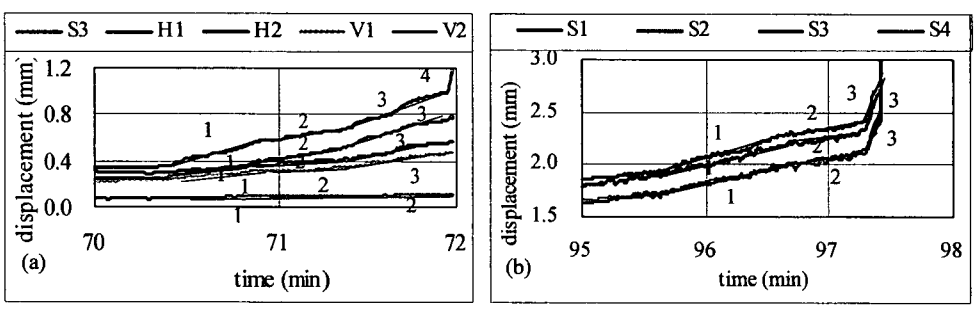

Figure 7. After failure (a) SH slope, (b) LH slope and laser sensors measurement (c) SH slope and (d) LH slope.

In the tests here, measurements made from SL and SSC tilt sensors as well as laser sensors were shown and compared. Here, for SL tilt sensors, only X-direction movement was measured whereas for SSC sensors, both X and Y direction movements were measured. In case of laser sensors, In case of laser sensors, slope surface movements measured were represented by S1, S2, S3 (from bottom upward) where as vertical and horizontal movements measured were represented by V1, V2 and H1, H2, respectively. In Figs. 6(a) and 6(b), movements of slope surface and slope top measured with laser sensors for SH and LH are shown. In case of Fig. 6(a), measurement of S1 and S2 were not good as the excavation reached the area of their set up positions after 6th cut onwards. In both the figures, almost no movement was seen at the beginning but the gradual increment with the increase in the steps of excavation could be measured from all the sensors. In case of SH slope, sharp increment was observed after 70 minutes. Similarly, in case of LH, sharp increment was observed after 95 minutes. In Figs. 7(a) and 7(b), measurements after 70 minutes for SH slope and after 95 minutes for LH slopes are shown. In both of those graphs, three curves were selected as shown in Fig. 7 and for each curve, inclination was measured. Change in the inclination (mm/min) for each curve is plotted in Figs. 8(a) and 8(b) for SH and LH slopes, respectively.

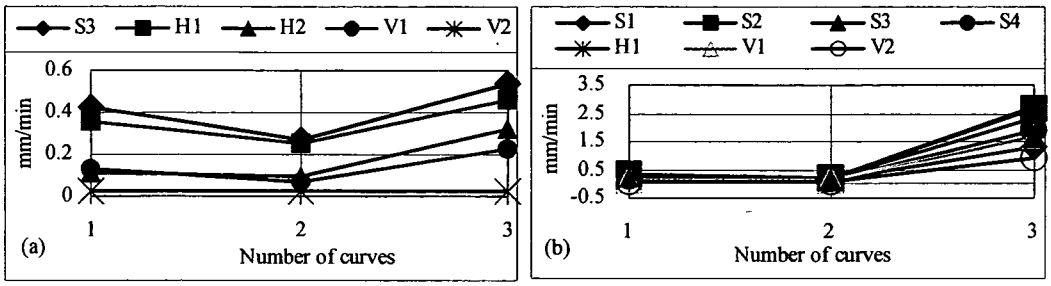

Figure 8. Measurement of laser sensors (a) SH slope and (b) LH slope.

In both the graphs, it could be observed that either the inclination of 2nd curve is little less than 1st curve or almost same where as the inclination of 3rd curve is comparatively very high. From this, it could be said that before reaching final failure, small decrement in inclination (or almost same) will take place after which sharp and final failure take place. This trend was observed in almost all the measurements made by laser sensors. One should be careful with this trend of change in increment. As seen from the graphs, the laser sensors which were set up near to the excavation portion, showed higher amount of change in the movement. Similarly, laser sensors set up toward the slope crest showed higher movement than those set up behind. Accordingly, S1 showed higher change in movement than those by S2, S3 and S4; S4 showing the minimum value. Similarly, on the slope top, H1 and V1 showed larger movement in comparison to H2 and V2, respectively.

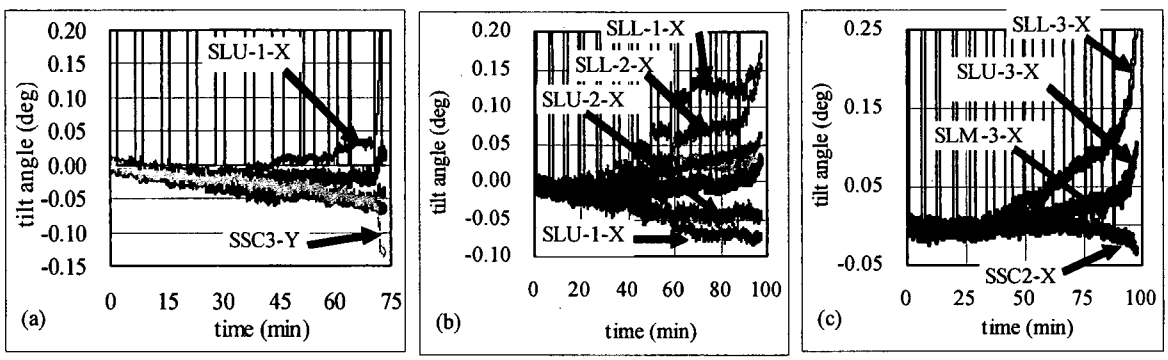

Figure 9. Measurements made from laser sensors (a) slope top (SH slope), (b) slope surface (LH slope) and (c) slope top (LH slope).

In Fig. 9, tilt angles measured on the slope surface and slope top for SH slope are shown. As the excavation reached the set up area of SSC-1 and SSC-2 tilt sensors after 6th cut, their data were not shown here. Hence, the measurement made on the slope top with SSC-3 (both X and Y movements) and SL-1 (X-direction only) and SL-2 (X-direction only) are shown. Although clear increments at the beginning of the excavation were not seen, change in the tilting angle could be seen with the increase in the steps of excavation. Just before the failure, i.e. after 70 minutes; sharp increment in the tilt angle was seen as those in laser sensors (Fig. 6(a)). Comparatively, the SL-1 and SSC-3 tilt sensors showed sharp change in their measurement just before the final failure. In case of SL-1, SLU-1 showed large tilting angle than SLL-1. For SSC-3 set up on the slope top (crest), positive movement along X direction and negative movement along Y direction, which was larger than X movement, were observed. From SSC-3 movement, it could be said that the slope had moved towards the right direction of the slope face during the failure. Similar failure pattern was seen during failure of the test also. Although no clear tensile crack or failure surface were appeared on the slope top, movements of SLU-1 and SLL-1 showed the possible measurement of slope movement of upper and inner layers. As shown in Table 2, SL-1 showed larger positive movement than SL-2 which showed very small negative movement only. Also, SLU-1-X showed larger movement than SLL-1-X, showing larger movement of upper layer than lower inner layer. Possible forward movement of the slope crest was hence occurred in the SH slope.

In Figs. 10(a) and (b), tilt angles measured for LH slope both by SL and SSC tilt sensors for the slope surface and slope top are shown, respectively. As in Fig. 7, here also, increments are not clear at the start with the increase in the step of excavation. But increment in tilt angle could be seen at the later stages of excavation; especially after 88 minutes of excavation, there was sharp increment in the tilt angle in all the cases. The increment became sharp when the elapsed time reached 95 minutes. In Fig. 10(a), comparing of the tilt angle measured by SL-1, SL-2 and SSC-1 are shown. SSC-1 showed positive X-direction movement only. Comparing the values of SL-1 and SL-2, all the SLL-1, SLM-1 showed higher positive values (X-direction) than SLL-2, SLM-2. In contrary, SLU-1 showed higher negative values (X-direction) than that by SLU-2. As SL-1 tilt sensor was set up closer to the excavation area, henceforth it showed the larger change in tilt angle than that by the SL-2 which was set up far away from the excavation area. It is to be pointed out here that the movement of all the sensors attached to SL-1 and SL-2 showed increment in tilt angles. This shows that the SL tilt sensor could measure the tilt angle of both upper and inner layers of the slope. As shown in Table 2, SL-1 and SL-2 both showed similar amount of movements; showing that whole the slope surface was moving forward, with the inner layer (SLL-1 and SLL-2) moving outward than the upper layers (SLU-1 and SLU-2). Since the inner layer movement angle